



# Synthesis, morphology, structural, and rheological studies of $\text{Fe}_{0.01}\text{Al}_{0.5}\text{La}_{0.01}\text{Zn}_{0.98}\text{O}$ -based polyaniline composite materials

M. Sohail<sup>1</sup> · M. Saleem Khan<sup>2</sup> · Muhammad Omer<sup>1</sup> · Ihsan Ullah Marwat<sup>1</sup> · Noor Saeed Khattak<sup>3</sup> · Sana Ullah Khan<sup>4</sup> · Zakir Ullah<sup>5</sup> · Sami Ur Rahman<sup>2</sup>

Received: 27 July 2017 / Revised: 12 April 2018 / Accepted: 17 May 2018 / Published online: 12 June 2018  
© Australian Ceramic Society 2018

## Abstract

In the present study, mixed-metal ceramic  $\text{Fe}_{0.01}\text{Al}_{0.5}\text{La}_{0.01}\text{Zn}_{0.98}\text{O}$  particles and their composites with polyaniline (PANI) were prepared via sol-gel and in situ free-radical polymerization techniques, respectively. Particles and composite formation was confirmed by FT-IR spectroscopy. SEM studies showed the  $\text{Fe}_{0.01}\text{Al}_{0.5}\text{La}_{0.01}\text{Zn}_{0.98}\text{O}$  particle's homogeneous dispersion in the polymer matrix. Ceramic particles were found to be in microdimensions. XRD analysis confirmed crystallite size in the range from 22 to 28 nm. Extensive rheological characterization was performed to check the durability of the materials for possible applications. Flow-curve tests suggested that the prepared materials are non-Newtonian (shear thinning) in nature. Increasing temperature have no appreciable effect on the viscosity which confirmed the mechanical stability of the materials. Based on frequency sweep test findings, the mechanical rigidity of the polymer has been enhanced ( $G' = 2 \times 10^2 - 5.22 \times 10^3$  Pa) by the introduction of ceramic particles. Conversely, creep compliance has been decreased considerably.

**Keywords** PANI composite · XRD · Rheology

## Introduction

The integration of inorganic fillers especially ceramic particles into a polymer matrix is of significant industrial importance. These reactive organo-ceramic composites have desirable properties adjusted to specific applications [1]. For the first time, these composites were produced in 1981 [2] to increase the flexural strength of cement. It was investigated that the combination of cement and polyvinyl alcohol (PVA) under high shear mixing produced hardened composites having

flexural strengths of about 200 MPa. Henceforth, an efficient number of combinations of fillers and polymers have been reported in literature [1, 3]. In the composites, both components (organic/inorganic) offer distinct features while modifying and reinforcing each other. Ceramic-based polymer composites can be synthesized at ambient temperature in the form of thick pastes that become hardened materials having similar characteristics like fired ceramics after low-temperature heat treatment. During high shear procedure, the physical and/or chemical interactions between ceramic and polymer phases result in the production of paste with enhanced rheological properties [3]. With progression of interactions, the paste becomes harder and its viscosity increases with time. Thus, it is important to recognize that during processing, how the rheology of paste changes with time.

Regardless of the type of ceramic used for strengthening the polymer matrix, rheological properties of the composite mostly depend on ceramic particle loading, their dispersion, and orientation in the polymer matrix and other processing parameters. It has been observed that with an increase in well-dispersed particle concentration in the polymer matrix, mechanical properties of composite increased [4]. Monolithic inorganic filler (ceramic) does not bear all required mechanical and other functional features. Therefore,

✉ M. Sohail  
msohail2000@gmail.com

<sup>1</sup> Institute of Chemical Sciences, University of Swat, Mingora, Khyber Pakhtunkhwa, Pakistan

<sup>2</sup> National Center of Excellence in Physical Chemistry, University of Peshawar, Peshawar, Pakistan

<sup>3</sup> Center for Material Sciences, Islamia College University, Peshawar, Pakistan

<sup>4</sup> Department of Chemistry, Women University Swabi, Swabi, Khyber Pakhtunkhwa, Pakistan

<sup>5</sup> Department of Physics, University of Malakand, Lower Dir, Khyber Pakhtunkhwa 18800, Pakistan

ceramic-based composite materials are prepared and increasingly utilized. Many methods are used for the preparation of ceramic polymer composites, but the prominent are sol-gel, direct mixing, and in situ polymerization [5]. Mixed-metal ceramics or ferrites ( $\text{FeMO}$ ) where M is generally a transition metal atom, are widely used in numerous technologies due to their interesting physical properties, versatility, and low cost. They deliver mechanical strength and colloidal stability when used as fillers with polymers in composites. It has been found that  $\text{MgFe}_2\text{O}_4$ /polyaniline (PANI) composites exhibit relatively better conductivity than pure  $\text{MgFe}_2\text{O}_4$  [6].  $\text{Cu}_{0.4}\text{Zn}_{0.6}\text{Cr}_{0.5}\text{Sm}_{0.06}\text{Fe}_{1.44}\text{O}_4$ /PANI composite due to its coercivity (comparatively lower than pure  $\text{Cu}_{0.4}\text{Zn}_{0.6}\text{Cr}_{0.5}\text{Sm}_{0.06}\text{Fe}_{1.44}\text{O}_4$ ) have been used as soft magnetic materials. Metal oxide  $\text{Fe}_2\text{O}_3$  intercalation in polypyrrole enhanced the conductivity of polypyrrole up to the order of  $10^{-2}$  [7]. Another reason for using metal oxide as filler in polymer matrix is reducing their agglomeration. Metal oxide particles are usually highly agglomerate, and if they are not kept dispersed by using a trapping or encapsulating media, they can coalesce very quickly. Therefore, to improve the surface state of metal oxide particles and make them chemically passive, bonding of capping agents (polymers) to metal oxide particles is necessary. This strategy is helpful in the decentralization and stabilization of metal oxide particles. The decrease in agglomeration has a significant effect on the optical and electrical properties of ceramic particles. Similarly, conducting polymers such as PANI and polypyrrole (PPy) are promising materials due to their attractive mechanical and electrical properties. Composites based on PANI have been investigated as potential high-performance electro-rheological materials with improved responses [8]. There exists a close relationship between the polymer processing steps and the rheology of the polymer. Hence, a good understanding is required about the fabrication steps of the composites and their rheological behavior.

The present study emphasizes on the rheological properties of mixed-metal ceramic-based PANI composite material. Metal oxide ceramic particles of almost the same composition have been used with neutral polymers viz. PVA/PEG/PVP for their electric, magnetic, and water purification properties [7]. We have studied the thermal and electrical properties of this composition in our previous work [9]. Up to the best of our knowledge, the existing literature is deficient in exploring the rheology and mechanical strength of such ceramic-based polymer composites. For this purpose, this particular composition was selected. Ceramic particles were prepared by sol-gel technique. The particles were used as fillers in PANI matrix via in situ free-radical polymerization. Rheology of the prepared materials was then studied via rheometry.

## Materials and methods

### Materials

Ferric nitrate ( $\text{Fe}_2(\text{NO}_3)_3 \cdot 9\text{H}_2\text{O}$ ) and zinc nitrate ( $\text{Zn}(\text{NO}_3)_2 \cdot 6\text{H}_2\text{O}$ ) were obtained from Scharlu (Spain), lanthanum nitrate ( $\text{La}(\text{NO}_3)_3 \cdot 9\text{H}_2\text{O}$ ) from Merck (Pakistan), aniline ( $\text{C}_6\text{H}_5\text{NH}_2$ ) from Acros Organics (USA), citric acid ( $\text{C}_6\text{H}_8\text{O}_7$ ) from Daejung (Korea), and potassium nitrate ( $\text{KNO}_3$ ), potassium permanganate ( $\text{KMnO}_4$ ), and ammonium per sulfate ( $(\text{NH}_4)_2\text{S}_2\text{O}_8$ ) from BDH (England). The chemicals were of analytical grade and were used without further purification. In all experiments, doubly distilled water (Millipore, USA) with electrical conductivity of  $0.51 \mu\text{S cm}^{-1}$  was used. Different experimental conditions such as concentration of the precursors, temperature of reactions, and pH of the solutions were optimized.

### Sample preparation

#### Preparation of mixed-metal ceramic particles

Ceramic particles comprising multi-metallic oxide ( $\text{Fe}_{0.01}\text{Al}_{0.5}\text{La}_{0.01}\text{Zn}_{0.98}\text{O}$ ) were prepared by sol-gel route. All the selected metal nitrates were taken in specific stoichiometric molar ratio and were dissolved in 100 ml doubly distilled water. Molar ratios of metal nitrates were calculated based on the total reducing and oxidizing coefficients, to get the equivalence ratio of unity and maximum energy release. The system was kept under vigorous magnetic stirring (500 RPM) for 2 h. During the experiment,  $\text{C}_6\text{H}_8\text{O}_7$  was admitted slowly to the solution to chelate the metal cations. For keeping the pH of the solution neutral, liquid ammonia ( $\text{NH}_4\text{OH}$ ) was added drop wise. After 2 h, the mixture was transferred to a drying oven where the temperature was set at  $80^\circ\text{C}$  for 90 min. During this interval, a light bluish gel was obtained which was sintered at  $600^\circ\text{C}$  in a furnace for 3 h. The solid diffused material obtained after sintering was cooled to room temperature and was converted to powder form. The ceramic sample was assigned a sample ID S1.

#### Preparation of ceramic-based PANI composite

Ceramic-based PANI composite was prepared by in situ free-radical polymerization. During the process, 250 mg of the prepared S1 particles was dispersed in 100 ml distilled water under magnetic stirring. In another set of experiment, 10% aniline solution in 1 M HCl and 0.1 M  $(\text{NH}_4)_2\text{S}_2\text{O}_8$  in 1 M HCl were prepared separately. Then 25 ml of each of these solutions were added drop wise to S1 parent solution. The whole reaction mixture was then processed under stirring for 3 h at low temperature ( $0\text{--}5^\circ\text{C}$ ). The mixture was then kept for digestion overnight to decrease the effect of

coprecipitation. The obtained material was then centrifuged at 4000 RPM for 10 min twice to remove side products and soluble impurities. The sample was finally dried for 2 h at 70 °C. The final product was named as S2.

## Characterization

Energy-dispersive X-ray (EDX) analysis was performed using X-ray Philips analytical diffractometer (US) attached with SEM. Samples with about 50 mm diameter (20 mm thick) were accommodated in the X-ray chamber of the machine. FT-IR analysis was done through Shimadzu (IR Prestige-21) spectrometer (Japan). A 5% solid solution of each sample with KBr in the form of thin pellets was prepared and analyzed. For structural analysis, the XRD patterns of the prepared samples were analyzed by JDX-3532 (JEOL JAPAN) X-ray diffractometer having a fixed radiation wavelength of  $\lambda = 1.54 \text{ \AA}$ . Each sample was sized to 1 in.<sup>2</sup> for XRD analysis. Rheological properties were analyzed using Anton Paar Rheometer (Physica MCR 301 Germany). The instrument comprises computerized motor drive employing plate-plate assessing system having automatic gap system, normal force measuring, and control sensors. Samples (5–10 mg) were placed between the plates. All measurements were carried out under internally controlled thermal conditions.

## Results and discussion

### Elemental composition of the prepared ceramic

The mixed-metal ceramic was investigated for its elemental composition by using EDX analysis. It was found that the material is composed of Fe, Al, La, and Zn elements. It is assumed that the material is of Fe- and La-substituted Zn/Al ferrite form. In the EDX spectrum (Fig. 1), peaks for silicon and sulfur were also observed which indicates that some traces of these elements are present in the material. This might be due to the careless handling of the S1 sample during preparation of pellets for EDX analysis. From Table 1, it is evident that the percentage composition is almost equal to the optimized starting stoichiometric composition selected for the preparation of the S1. The composition of S2 was predicted from the FT-IR studies where different peaks represent functionalities corresponding to different functional groups in PANI chains and metal oxides in functional group and fingerprint regions, respectively. The intercalation of S1 particles in PANI chains was also confirmed by the smooth morphology of S2 in SEM analysis. These results will be discussed in the subsequent sections.

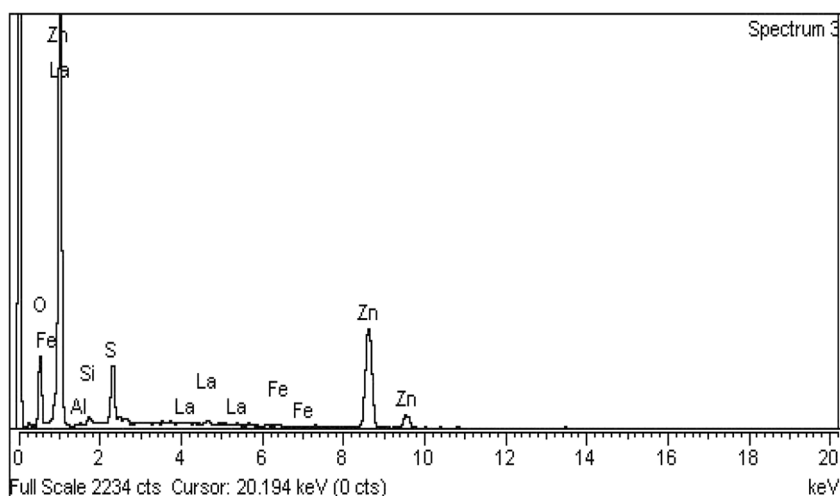
### Functional group analysis

FT-IR spectroscopy was performed to investigate the synthesis of S1 particles and their compositing with PANI in S2. Metal oxides generally display IR peaks in the fingerprint region ( $< 1000 \text{ cm}^{-1}$ ) which arises due to inter-atomic vibration. A dense series of absorption peaks has also been observed in this region which is assigned to bending vibrations of the particles. A broad peak at  $3370 \text{ cm}^{-1}$  in S1 spectrum (Fig. 2) is assigned to the O–H stretching modes due to the adsorption of water molecules on the metal surfaces [10]. Another transmission peak at  $1600 \text{ cm}^{-1}$  may also be due to the absorbed water from air during KBr pellet formation. Zn–O stretching vibration in S1 is represented by a sharp absorption band at  $460\text{--}480 \text{ cm}^{-1}$  while Fe–O stretching vibration is denoted by a strong absorption peak at about  $600 \text{ cm}^{-1}$  in the S1 spectrum. Two small peaks obtained at  $420$  and  $2330 \text{ cm}^{-1}$  are ascribed to metal-oxygen complexes. FT-IR spectrum of S2 (Fig. 2) approves the development of composite of S1 particles in PANI matrix. A broad band at about  $3506 \text{ cm}^{-1}$  exhibits the O–H stretching and deformation mode in S2 composite. Various modes of C–C, C–H, and C–N functionalities in S2 are represented at  $621$ ,  $1070$ ,  $1284$ , and  $1480 \text{ cm}^{-1}$ , respectively. Peak at about  $3005 \text{ cm}^{-1}$  is allocated to the symmetric stretching of methyl and methylene groups in the S1-PANI (S2) composite. The absence of any clear peak in the region from  $2800$  to  $1600 \text{ cm}^{-1}$  in S2 shows the absence of O–H mode, C=H, and C–O stretching mode of organic sources in the material in this region which reveal the effective dispersion of ceramic particles in the polymer matrix [11]. This also confirms that the free functionalities of PANI have been occupied by the S1 particles in the S2 composite.

### Morphology

SEM techniques identified the surface texture of S1 and S2 materials. SEM micrograph (Fig. 3a) of S1 reveals that the ceramic contains spherical and rod-shaped crystallites with particle size ranging from  $0.5$  to  $5 \text{ \mu m}$ . It indicates the polycrystalline nature of S1 sample. The crystallites were formed on cooling of S1 after sintering at  $600 \text{ °C}$ . Agglomeration in little extent was also observed in S1 micrograph which is assumed to be due to the solvent effect. In the metal oxides, the oxygen atom interacts with the hydrogen atoms of water via H bonding thus resulting in the close packing of particles and hence agglomeration [11]. During sintering the sample, thermal strain also produced some pores on the surface which are considered important in crystallites for their cell in-growth. The SEM micrograph of S2 (Fig. 3b) represents well-dispersed ceramic particles in polymer matrix without forming any large aggregation. S2 surface is nearly smooth and displays no visible defects for example large pores which specify that S1 particles interacted through stable cohesive bonds with

**Fig. 1** EDX spectrum of S1 ceramic particles



PANI chains. The S1 particles are firmly immobilized in the polymer matrix and seem not to be self-connected. Ceramic particles seemed to be smaller in size as compared in Fig. 3a. The reason is that the ceramic particles are embedded in the polymer chains which shade either totally or some of the portion of the particles which internally reflects the small size of the particles. However, the particles retain their original size within the matrix. Such type of composite morphologies is preferred in applications like high-energy density media and capacitors.

### XRD analysis

Phase analysis and crystallinity of the ceramic particles and its composites were investigated via XRD. The XRD patterns for S1 and S2 are shown in Fig. 4. The well-resolved peaks in S1 pattern confirm the monophasic nature of the ceramic particles which signifies the absence of any secondary phase. The S1 peaks are well indexed to the equivalent crystallographic planes at (100), (101), (002), (102), (113), (103), (110), (200), and (112), which illustrate the hexagonal wurtzite ZnO-like structure with P 63mc space group as predictable from JCPDS card file No. (30-1451) [12]. The undefined small peaks in the S1 pattern denote the noise which is prescribed to the instrumental alignment during XRD analysis. S2 pattern represents some additional peaks at  $2\theta = 14^\circ$  and

$25^\circ$ , representing the presence of PANI in the composite and the dispersion of particles in its chains [12]. Both of these peaks match with (200) and (110) crystallographic planes, respectively, which show the scattering of X-rays from PANI. Other peaks at high  $2\theta$  are linked with diffraction from ZnO planes which are retained in the composite. It is also evident that some peak intensities diffracting at  $2\theta = 31.65^\circ$ ,  $34.35^\circ$ ,  $36.15^\circ$ ,  $47.55^\circ$ , and  $56.45^\circ$  with corresponding (100), (101), (110), (002), and (103) planes have been suppressed and occupied at different ratios. This demonstrates the interaction between S1 particles and PANI chains. The composite adopts a semi-crystalline nature. The intensity of peak at  $2\theta = 65^\circ$  has been increased in S2 which is attributed to the uniform dispersion/distribution of S1 particles in PANI matrix [5]. It is also assumed that S1 particles act as nucleation sites for PANI chains which ultimately increase the crystallite size of the composite. This may also be attributed to the accumulation and increase in volume content of S1 particles in PANI matrix, resulting in the microstrain in the composite. The average crystallite size of S1 and S2 was assessed using Scherer's

**Table 1** Percent elemental composition of S1 ceramic particles

Name of element	Atomic %	Weight %
Zn	43.52	71.60
The	0.41	1.45
Al	0.48	0.32
Fe	0.40	0.57
S	8.43	6.81
O	45.34	18.26

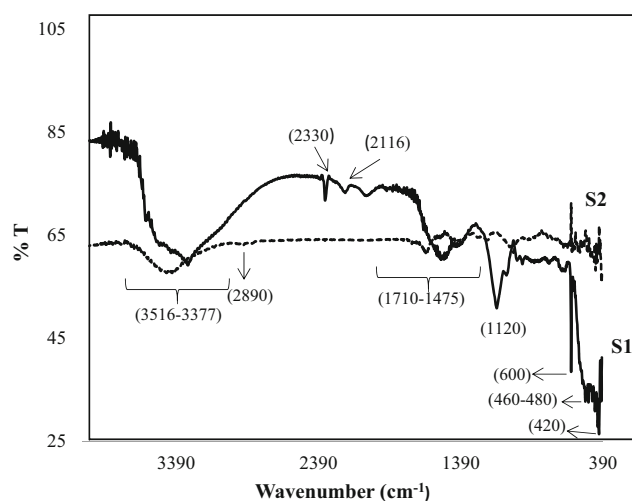
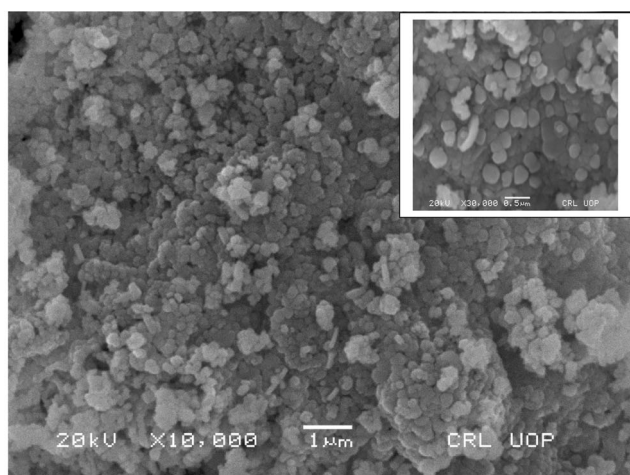
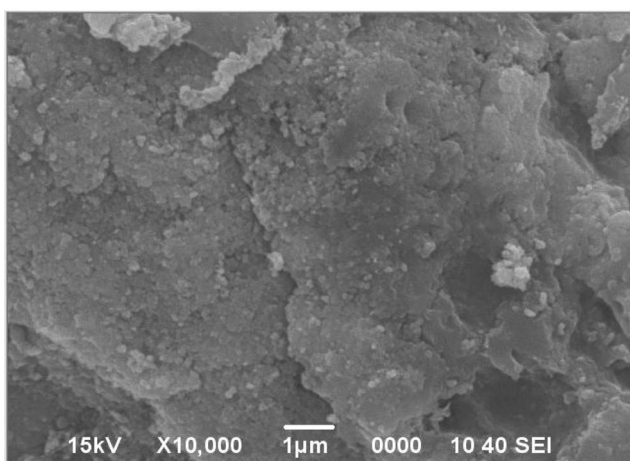


**Fig. 2** FT-IR spectra for S1 and S2 samples



a



b

Fig. 3 SEM micrographs for a S1 particles and b S2 composite

formula (Eq. 1) from the full width at half maximum (FWHM) of the maximum intensities in the patterns.

$$t = \frac{k\lambda}{\beta \cos\theta} \quad (1)$$

where  $t$  is the crystallite size,  $k = 0.9$ ,  $\lambda = 1.54 \text{ \AA}$ , and  $\beta$  is the FWHM. The average crystallite size of the particles measured was 22 nm for S1 and 28.35 nm for S2 with a lattice strain of about 0.0053 and 0.0059, respectively. The materials in this range of crystallite size are suitable for high-energy density media. As mentioned in SEM analysis, the particle size is in the range from 0.5 to 5  $\mu\text{m}$ . This also confirms the combination of nano-crystallites to produce large particles. From XRD studies, a mechanism of composite formation between S1 particles and polymer can be assumed. PANI acts as a capping agent while metal ions in S1 act as precursors. The trivalent ions (iron and lanthanum) and divalent ion (zinc) make strong ionic interaction with amide groups of the PANI chains. Accordingly, a constant immobilization of metallic ions occurs in the cavities of polymer chains. Thus, a solid solution of

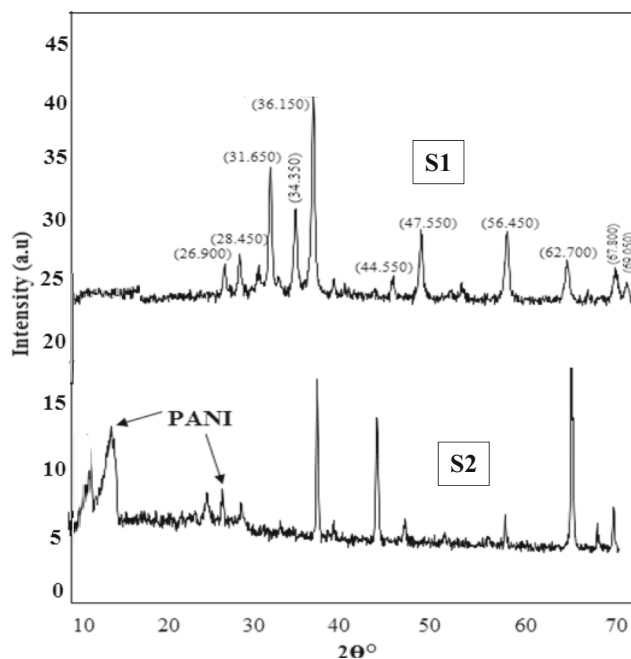


Fig. 4 XRD patterns for S1 particles and S2 composite

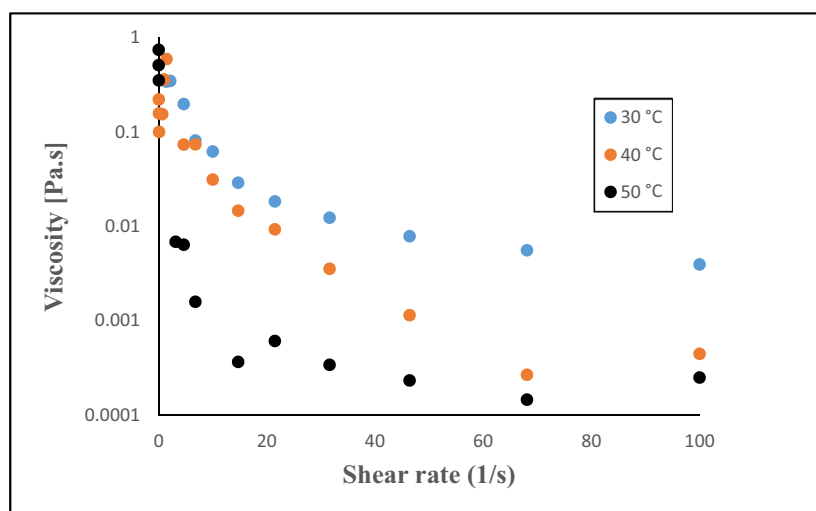
uniformly distributed metal oxides inside the PANI matrix is produced. This behavior is denoted by the vanishing of some peaks with low intensities in the composite (S2).

### Mechanical properties (rheology)

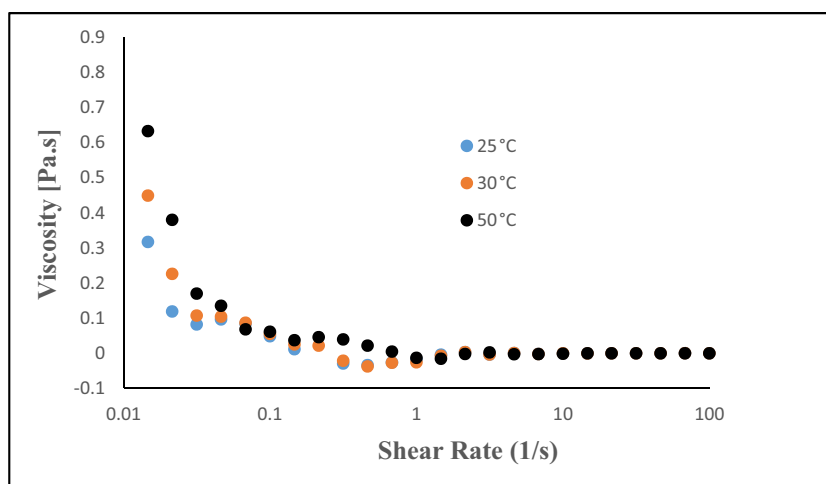
#### Flow curves

Flow curves between shear rate and viscosity (Fig. 5a) were recorded at three different temperatures (30, 40, and 50 °C). It is evident that S1 viscosity ( $\eta$ ) decreased with increasing shear rate ( $\dot{\gamma}$ ) at all temperatures which indicates the shear thinning or non-Newtonian behavior of S1 particles. No constant viscosity regime is observed either at low and higher shear rates. It is assumed that at low shear rates, the interactions among the metal ions present in the mixed ceramic S1 cannot be disintegrated and it is hard to flow. But with increasing shear rate, interatomic interactions become weak and thus structure break down and deformation arise that ultimately result in the reduction of viscosity of S1 compact system [2]. It should be noted that rheological measurements became difficult for  $\dot{\gamma}$  above 100  $\text{s}^{-1}$  due to macroscopic aggregate formation and instabilities in ceramic particles. Figure 5b represents the flow curve for S2 composite. It is evident that  $\eta$  of the composite is inversely proportional to the applied  $\dot{\gamma}$ . The decreases in  $\eta$  is attributed to the weakening of interactions established among PANI chains and ceramic particles. The curve plot demonstrates that S2 composite shows highest value of  $\eta = 0.63 \text{ Pa s}$  at 0.015  $\text{s}^{-1}$   $\dot{\gamma}$ . This implies that S1 particles have been well-dispersed in polymer matrix [13]. The decrease in  $\eta$

**Fig. 5** Flow curves at three different temperatures: **a** S1 sample and **b** S2 composite



**a**



**b**

with increasing  $\gamma$  specifies the shear thinning and non-Newtonian character of the composite. It is ascribed that low  $\gamma$  is incapable of breaking the induced structure of S2; however, as  $\gamma$  increases, the induced structure in S2 disintegrates and flow of materials occurs. The composite S2 shows Newtonian behavior at low shear rates with a zero-shear viscosity ( $\eta_0$ ); at intermediate  $\gamma$ , viscosity decreases while following a shear-thinning behavior and at high  $\gamma$ , the viscosity reaches a limiting value, i.e., infinite-shear viscosity ( $\eta_\infty$ ). This implies that the composite exhibits pseudo-plastic behavior. It has also been reported in literature that the decrease in  $\eta$  at increasing  $\gamma$  is either due to orientation of suspended ceramic particles in the direction of flow or to the shear thinning behavior of the polymer matrix [13]. Upon the dispersion of ceramic particles in PANI matrix, the viscosity of S1 decreased from 1.5 to about 0.85 Pa s under a  $0.01\text{-s}^{-1}$  shear rate, which shows the ability of PANI to act as a rheological convertor with a thinning action on S1 particles. In addition to

a thinning effect, the enhanced stability of S2 composite in the rheological measurements proposes that PANI chains also have a stabilizing action on S1 particles, limiting their reshuffling and hence aggregation. This also confers that the shear-induced arrangement of PANI network is not impacted by the S1 particle addition. This is in accordance with the fact that both S2 composite and pure S1 particles present a similar rheological behavior. The S2 composite presents a compatible viscosity and shear thinning behavior for applications like screen printing [14]. It was also observed that in both cases, no significant change in viscosity occurs with increasing temperature thus presenting the significant stability of S1 and S2 toward temperature.

### Theoretical modeling

To check whether our experimental data is in coherence with theoretical proofs, different rheological models (Fig. 6a, b)

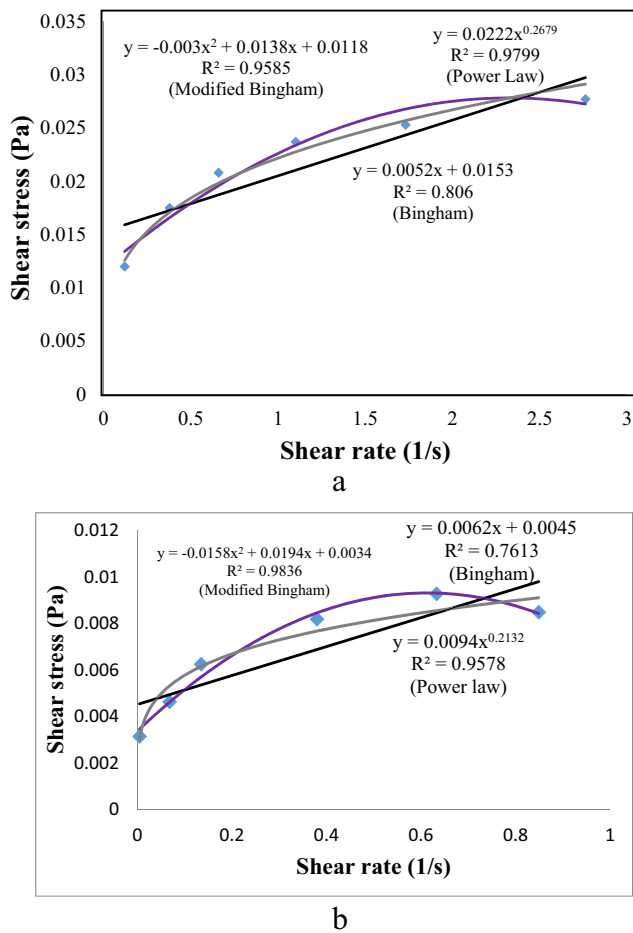


Fig. 6 Application of theoretical models to flow curves data: a S1 and b S2 samples

viz. Bingham (Eq. 2), modified Bingham (Eq. 3), and Ostwald power law (Eq. 4) [15] were applied.

$$\tau = \tau_0 + \eta_0 \gamma \tag{2}$$

$$\tau = \tau_{MB} + \mu_{MB} \gamma + Cr^2 \tag{3}$$

$$\tau = K\eta^{n-1} \tag{4}$$

where  $\tau$  is the shear stress,  $\eta_0$  is zero field viscosity,  $\tau_0$  is yield stress,  $\gamma$  is shear rate,  $C$  is constant,  $K$  is consistency co-efficient, and  $n$  is power law index. Bingham model tells about the flow properties of materials while modified Bingham and Ostwald power law show the shear thinning and mechanical rigidity of the materials. The correlation co-efficient ( $R^2$ ) values obtained from all the three models are listed in Table 2. It is evident that modified Bingham and Ostwald power law models are best fit to the data of S1 and S2 with  $R^2$  value in the range from 0.957 to 0.983. This shows the compatibility of experimental data with theoretical proof where both the observations represent the shear thinning behavior of the material under study. The power

Table 2  $R^2$  obtained from different rheological models for S1 and S2

Sample code	Bingham $R^2$	Modified Bingham $R^2$	Ostwald power law $R^2$
S1	0.806	0.958	0.979
S2	0.761	0.983	0.957

law/flow index ( $n$  = rate of change of structure with increasing shear rate) was also analyzed which denotes the level of dispersion for S1 particles in PANI matrix. The value of  $n$  for S1 = 0.26 and for S2 = 0.21 is significantly lower than 1, indicating a distinct shear thinning (non-Newtonian) behavior of S1 and S2 as predicted from the plots in Fig. 6a, b. It has been reported in literature that for stronger and tough materials, the  $n$  value is smaller [9]. In this sense, S2 shows more toughness as compared with S1 confirming the dispersion of S1 particles in PANI chains and hence the improvement of mechanical rigidity of S2

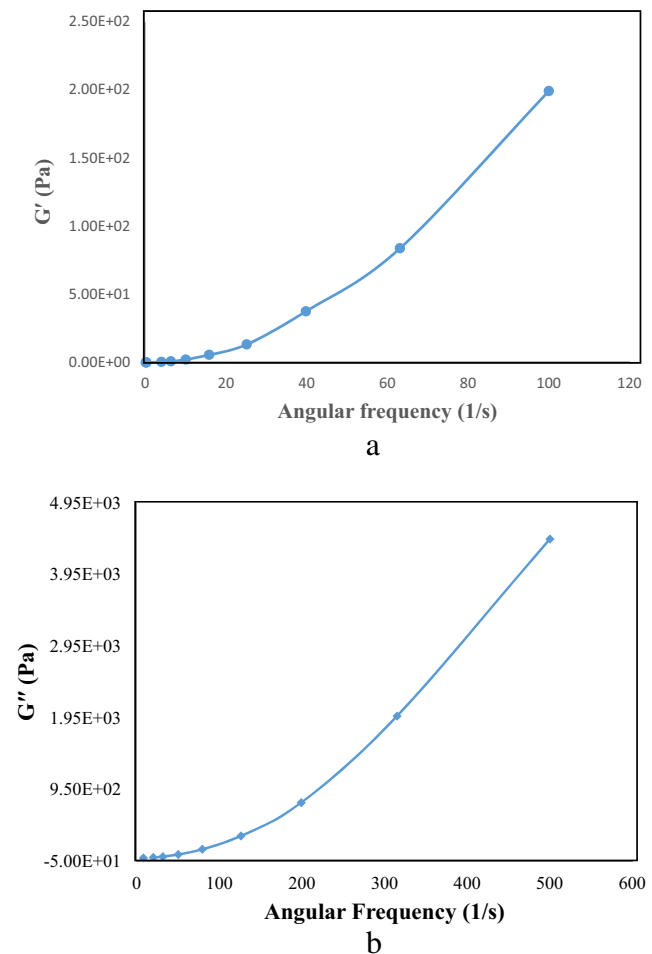
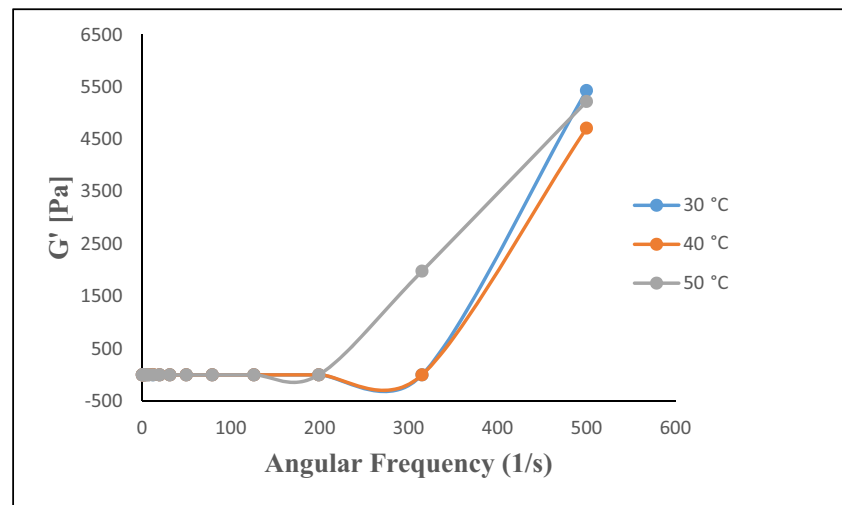
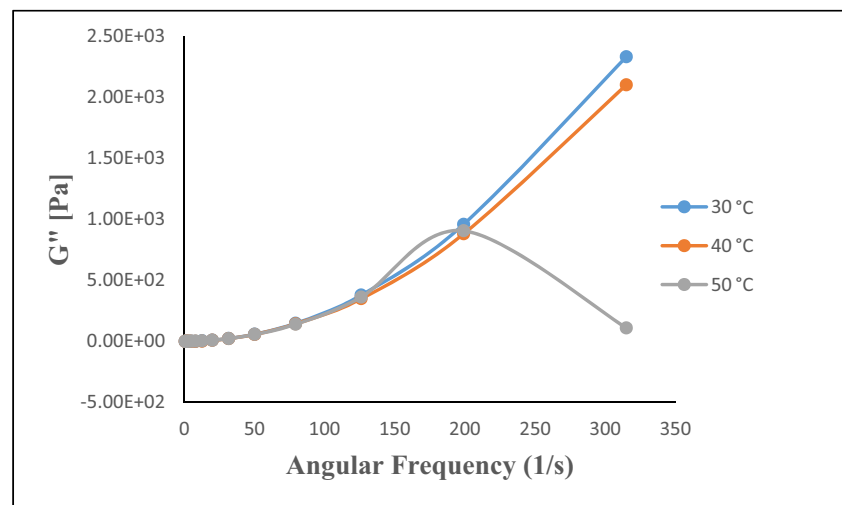


Fig. 7 Variation of  $G'$  and  $G''$  with angular frequency for S1 sample at a specific temperature

**Fig. 8** Variation of  $G'$  and  $G''$  with angular frequency for S2 composite at three different temperatures



a



b

composite. Based on this, the materials under study can be applied where tough membranes are required.

### Frequency sweep tests

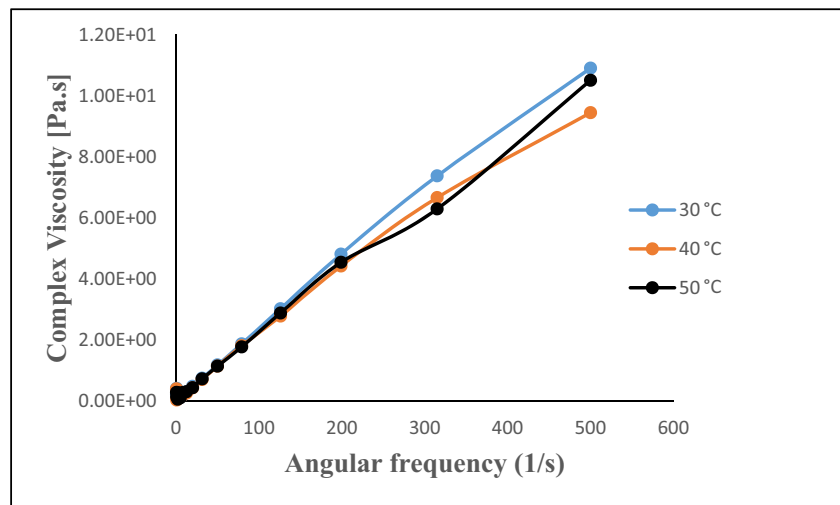
While analyzing rheological properties, frequency sweep analysis gives us information regarding the storage shear modulus ( $G'$ ), loss modulus ( $G''$ ), and complex viscosity ( $\eta^*$ ) of the material under study. The value of  $G'$  and the  $G''$  describes shear thinning, mechanical rigidity, and viscoelastic properties of the materials. They can also deduce the solid and liquid behavior of the materials. Figure 7a, b illustrates the linear relation between angular sweep frequency and both  $G'$  and  $G''$ . The increasing trend of  $G'$  and  $G''$  demonstrates the shear thinning (non-Newtonian) and better elastic nature of S1 particles [16]. The different metal ions in S1 ceramic composition are strongly bound to

one another, and they resist dislocation while acting like unchanging networks. Figure 8a, b and denotes the variation of  $G'$  and  $G''$  with angular frequency for S2 at different temperatures. It is obvious from the plots that  $G'$  for S2 has improved up to  $5.22 \times 10^3$  Pa relative to S1 ( $G' = 2 \times 10^2$ ). This shows the better dispersion of S1 particles in the PANI matrix [17]. However,  $G''$  is approximately equal for both the samples. Increase in  $G'$  also means that the composite's elasticity is greater which shows the mechanical rigidity and hence stability of the material. The complex modulus ( $G^*$ ) is representative of the material rigidity in terms of storage and loss moduli components according to Eq. 5.

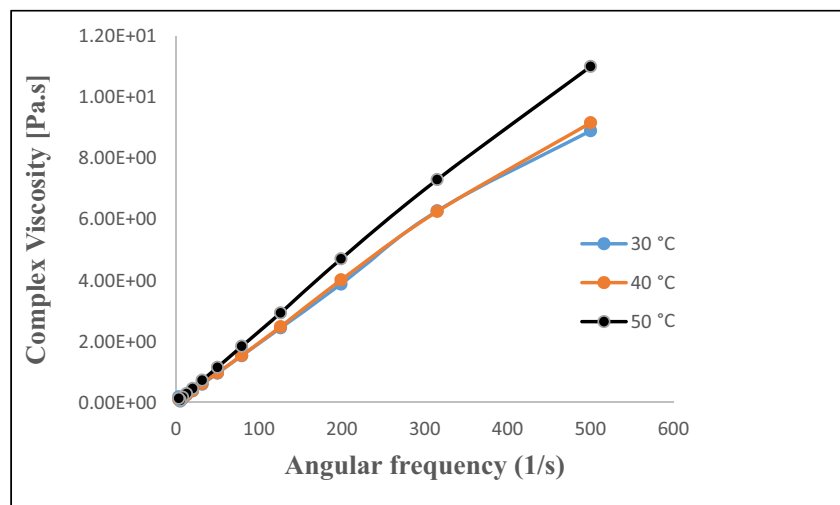
$$G^* = G' + iG'' \quad (5)$$



**Fig. 9** Complex viscosity versus angular frequency plots: **a** S1 and **b** S2 samples



**a**



**b**

The viscoelastic performance for S1 and S2 can also be determined while using the loss factor  $\tan(\delta)$  according to Eq. 6.

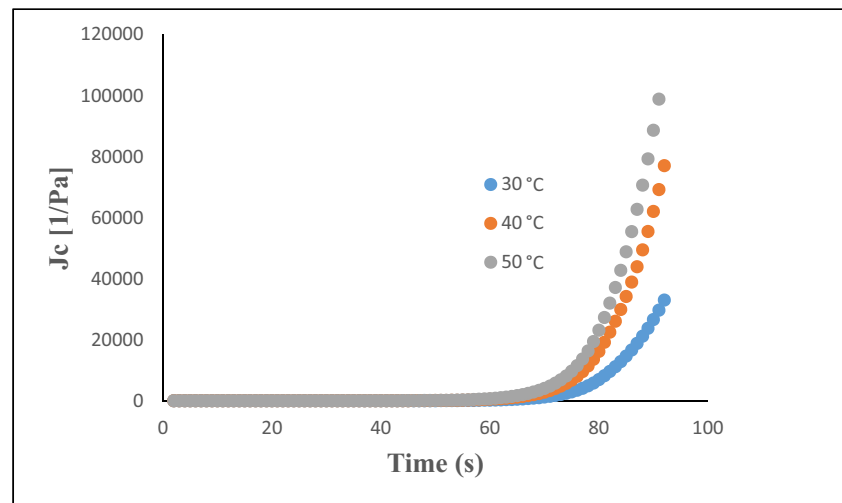
$$\tan\delta = G''/G' \tag{6}$$

From Eq. 6, it can be assumed that when the loss factor is greater than 1, the loss modulus will dominate and the material would have a dominant liquid behavior. On the other hand, when  $\tan\delta$  is smaller than 1, the storage modulus will dominate and the material would rather have a solid behavior. Here, in our case, the  $\tan\delta$  value obtained for S1 and S2 is in the range from 0.31 to 0.38 which confirms the solid behavior of ceramic particles and the composite.

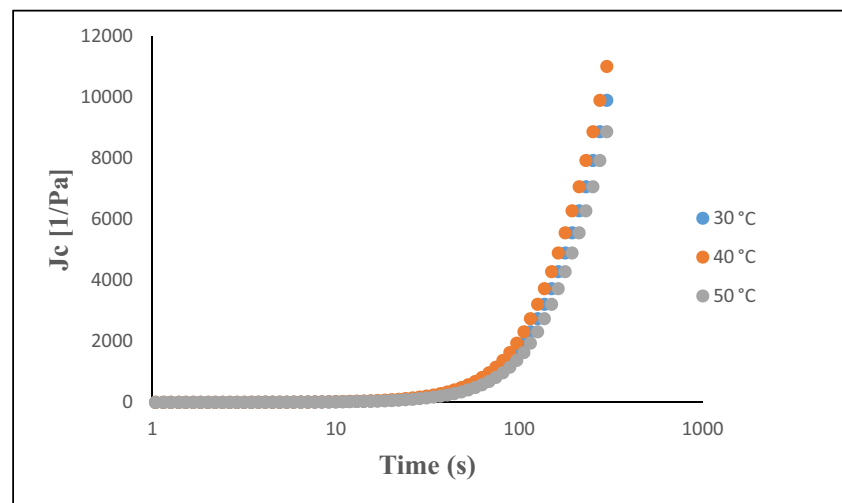
### Complex viscosity

Another rheological parameter known as complex viscosity can also be deduced from frequency sweep analysis. Angular frequency ( $\omega$ ) dependence complex viscosity ( $\eta^*$ ) for samples S1 and S2 is shown in Fig. 9a, b, respectively, at three different temperatures. Complex viscosity for S1 first decreases up to 3–5  $\text{rad s}^{-1}$  and then shoots up and touches a maximum value (10 Pa s). The drop in complex viscosity shows the shear thinning behavior of the S1 sample which is in agreement with Cox-Merz rule that correspondently occurs between the shear viscosity ( $\eta$ ), plotted against shear rate (Fig. 5), and complex viscosity ( $\eta^*$ ) plotted against  $\omega$  [18]. At this time, the interactions among the ions of S1 particles become weak but at high  $\omega$ , the dipoles attract each other through physical and chemical links and hence the material adopts a compact structure. Consequently, S1

**Fig. 10** Creep compliance with time plots: **a** S1 and **b** S2 samples



a



b

shows deviation from the rule at high  $\omega$  unlike polymeric melts. For S2 composite, complex viscosity shows an equilibrium position at low  $\omega$ , however, it rises up with increasing frequency. This shows the relaxation of polymer chains in S2 which limits the free mobility of metal ions in the matrix. The highest value of  $\eta^*$  for S2 is 10.90 Pa s which is almost similar to that of S1. Again, both the materials show stability toward increasing temperature as there is no such appreciable change that occurs in this property.

### Creep tests

Creep compliance ( $J_c$ ) is the reciprocal of the shear modulus ( $J = 1/G$ ) which is imagined as rigidity of a material. Both the prepared materials were checked for their viscoelastic behavior while performing  $J_c$  test as function of time at different temperatures. Figure 10a, b shows the creep compliance values for S1 and S2 samples. As estimated, integration of S1 particles increases the creep compliance of polymer in

**Table 3** Summary of different rheological parameters for S1 and S2

Sample code	$ \eta $ (Pa s)	$G'$ (Pa)	$G''$ (Pa)	$ \eta^* $ (Pa s)	$n$	$J_c$ (1/Pa)
S1	1.90	$2.00 \times 10^2$	$4.45 \times 10^3$	10.00	0.26	$9.8 \times 10^4$
S2	0.80	$5.22 \times 10^3$	$2.33 \times 10^3$	11.00	0.21	$1.1 \times 10^4$

the composite. It is interesting to note that S2 composite displays a lower creep in the whole time range. This finding agrees with literature [19]. The results suggest that creep behavior is a suitable indicator for the dispersion state of the S1 particles in PANI matrix. However, it is assumed that decrease in  $J_c$  for S2 is due to the reduced crystallinity of S1 particles while making composite with PANI, as reported earlier [20]. It is also reasonable to assume that the interactions between PANI chains and S1 particle surfaces become weaker when the higher stresses are applied. Therefore, as evident from the plots (Fig. 10b) that the S2 composite owes a glassy (compact) nature at initial stages and then with increasing time (at about 100 s) becomes viscoelastic. The creep results can be explained by considering the morphological differences between S1 and S2, as shown in Fig. 3a, b. Ceramic S1 is in particulate form while S2 composite has a smooth bulky morphology. Considering the external mechanical filling that includes changes in the semi-crystalline nature of the polymer, first chain rotation and separation take place when the amorphous PANI is stretched highly in the linear viscoelastic (creep) range. The S1 particles, being inserted in PANI chains strengthen the amorphous phase. Consequently, the stretching of the entangled and amorphous PANI chains in S2 composite occurs with significant time delay under the same load in the presence than in the absence of S1 particles. The result is the decreased creep and creep rate of the composite. Summary of different rheological parameters for S1 and S2 is shown in Table 3.

## Conclusions

In this study, we examined the effect of mixed-metal ceramic particles on the PANI polymer for different properties. Ceramic particles were synthesized by sol-gel method and then were introduced in the polymer matrix via in situ free-radical polymerization technique. Different physical properties with special emphasis on the rheological behavior of the materials were investigated. Based on FT-IR analysis, ceramic particles combined with PANI chains successfully in the composite. SEM analysis showed the homogeneous dispersion of the particles in the polymer matrix. XRD analysis showed the crystalline structure of the prepared materials. Rheological measurements showed that the materials exhibit Newtonian behavior at low shear rates while becoming non-Newtonian at high shear rates with stable performance toward increasing temperature. Experimental work was also proved by applying different theoretical models. Ceramic particle insertion in the polymer matrix have improved the mechanical rigidity ( $G' = 5.22 \times 10^3$  Pa) of PANI in the composite. The incorporation of ceramic particles in PANI have decreased creep compliance of the composite which confirms the dispersion of particles in the polymer.

**Acknowledgements** Mr. Majid Khan and Mr. Muhammad Irfan are also acknowledged for their support during the completion of this project.

**Funding information** The authors are thankful to the National Centre of Excellence in Physical Chemistry, University of Peshawar for financial support and to the University of Swat for providing a place to conduct this research work.

## Compliance with ethical standards

**Conflict of interest** The authors declare that they have no conflict of interest.

## References

- Chir-Jang, T., Chun-Nan, C., Wenjea, T.J.: Flexural strength and porosity of cements. *J. Eur. Ceram. Soc.* **33**, 3177–3184 (2013)
- Birchall, J.D., Howard, A.J., Kendall, K.: Rheological properties of ferrite nanocomposites based on nylon-6. *Nature*. **289**, 388–390 (1981)
- McHugh, A.J., Walberer, J.A.: Rheology, structure, and sintering of zirconia suspensions with pyrogallol-poly(ethylene glycol) as polymeric surfactant. *Compos. Part A*. **32**, 1085–1093 (2001)
- Faiz, S., Anis, A., Luqman, M., Al Zahrani, S.M.: Studies on thermal, mechanical, morphological and viscoelastic properties of polybenzimidazole fiber reinforced high density polyethylene composites. *Polym. Compos.* (2016). <https://doi.org/10.1002/pc.23148>
- Moeen, S.J., Vaezi, M.R., Yousefi, A.A., Ghasemi, E.: Synthesis and rheological properties of nickel-zinc ferrite polymer nanocomposites. *J. Appl. Polym. Sci.* **123**, 2534–2539 (2011)
- Khafagy, R.M.: Synthesis, characterization, magnetic and electrical properties of the novel conductive and magnetic polyaniline/MgFe<sub>2</sub>O<sub>4</sub> nanocomposite having the core-shell structure. *J. Alloys Compd.* **509**, 9849–9857 (2011)
- Ahmad, M.A., Khafagy, R.M., Bishay, S.T., Saleh, N.M.: Effective dye removal and water purification using the electric and magnetic Zn<sub>0.5</sub>Co<sub>0.5</sub>Al<sub>0.5</sub>Fe<sub>1.46</sub>La<sub>0.04</sub>O<sub>4</sub>/polymer core-shell nanocomposites. *J. Alloys Compd.* **578**, 121–131 (2013)
- Young, D.K., Yoon, D.J.: Synthesis and rheological properties of nickel-zinc ferrite polymer nanocomposites. *Korea-Aust. Rheol. J.* **28**(4), 275–279 (2016)
- Saleem, M.K., Sohail, M., Saeed, N., Ayesha, A.: Synthesis and characterization of three-phase polymer-graphene oxide-ceramic composites. *J. Chem. Soc. Pak.* **38**(2), 234–241 (2016)
- Kumar, H., Rani, R.: Structural and optical characterization of ZnO nanoparticles synthesized by microemulsion route. *Int. Lett. Chem. Phys. Astron.* **14**, 26–36 (2013)
- Goodarz, N.M., Elias, B.S., Hossein, A.A., Shaari, A.H., Hashim, M.: Simple synthesis and characterization of cobalt ferrite nanoparticles by a thermal treatment method. *J. Nanomater.* **2010**, 1–8 (2010)
- Kant, S., Kalia, S., Kumar, A.: A novel nanocomposite of polyaniline/Fe<sub>0.01</sub>Ni<sub>0.01</sub>Zn<sub>0.98</sub>O: photocatalytic, electrical and antibacterial properties. *J. Alloys Compd.* **578**, 249–256 (2013)
- Mohamed, K.R., Mousa, S.M., El Bassyouni, G.T.: Fabrication of nano structural-biphasic-materials from phosphogypsum waste and their in vitro applications. *Mater. Res. Bull.* **50**, 432–439 (2014)
- Chae, D.W., Lee, K.H., Kim, B.C.: Rheological properties of ferrite nanocomposites based on nylon-6. *J. Polym. Sci. B Polym. Phys.* **44**(2), 371–377 (2006)
- Fanny, H., Aurore, D., Nadège, R., Guillaume, K., Julien, B.: Rheology of cellulose nanofibrils/silver nanowires suspension for

- the production of transparent and conductive electrodes by screen printing. *Appl. Surf. Sci.* **394**, 160–168 (2017)
16. Zhang, X., Shen, L., Wu, H., Guo, S.: Enhanced thermally conductivity and mechanical properties of polyethylene (PE)/boron nitride (BN) composites through multistage stretching extrusion. *Compos. Sci. Technol.* **89**, 24–28 (2013)
  17. Saleem, M.K., Sohail, M., Saeed, N.K., Sayed, M.: Industrial ceramic waste in Pakistan: valuable materials for possible applications. *J. Clean. Prod.* **139**, 1520–1528 (2016)
  18. Prashantha, K., Soulestin, J., Lacrampe, M.F., Krawczak, P., Dupin, G., Claes, M.: Masterbatch-based multi-walled carbon nanotube filled polypropylene nanocomposites: assessment of rheological and mechanical properties. *Compos. Sci. Technol.* **69**(11), 1756–1763 (2009)
  19. Siengchin, S., Karger-Kocsis, J.: Structure and creep response of toughened and nanoreinforced polyamides produced via the latex route: effect of nanofiller type. *Compos. Sci. Technol.* **69**, 677–683 (2009)
  20. Selim, G., Weihua, L., Melih, K.C.: The rheology of shear thickening fluids with various ceramic particle additives. *Mater. Des.* **104**, 312–319 (2016)